Low-Loss Optimization and Collision Dynamics Analysis of the Feeding Hopper in the Oyster Seedling Dispensing Device

Jiaqi Han[1,a] and Yu'e Yang[2,b*]

[1]University of Jinan, School of Mechanical Engineering, Jinan 250022, China
[2]Shandong Key Laboratory of Surface Engineering and Intelligent Equipment for Key Metal Components, University of Jinan, Jinan 250022, China

[a]812762263@qq.com, [*b]me_yangye@ujn.edu.cn

Abstract. Shell damage of oyster spat during mechanized grading and cage division is a key factor limiting the practical adoption of automated aquaculture equipment. Taking the feeding hopper of an oyster seedling dispensing device as the object, this study develops a contact-dynamics simulation framework for low-damage structural design. Four hopper profiles—straight-wall, polyline, arc, and reverse-arc—are compared using an improved mass flow index (MFI), which accounts for both outlet-time dispersion and velocity dispersion, and a comprehensive damage index (D), which combines wall, inter-particle, and cumulative collision forces. The reverse-arc hopper exhibits the best overall performance, with an MFI of 0.562 and a D of 0.002, indicating uniform discharge and reduced collision risk. A parametric analysis of the reverse-arc central angle from 45° to 75° reveals a U-shaped wall-force response, with the minimum simulated wall collision force of 15.359 N at 50°. These results clarify how concave wall curvature regulates particle trajectories and energy dissipation, providing a design basis for low-damage conveying of oyster spat. Future work will include physical prototype tests and validation under varying operating conditions, oyster sizes, and feed rates to confirm practical robustness.

Keywords: oyster spat, feeding hopper, mass flow index, damage index.

1 Introduction

Mechanical damage during the mechanized handling of oyster spat is a practical bottleneck in the automation of aquaculture grading and cage division. Because oyster spat have thin, brittle, and irregular shells, improper impact or compression may cause shell-edge chipping, crack initiation, or complete fracture[1-2]. Reducing the mechanical stimulus below the damage threshold is therefore essential for the design of reliable seed-handling equipment.

The feeding hopper is one of the key components that governs the motion state of the particle population before it enters the grading or dispensing mechanism. Existing hopper and silo theories mainly target ores, grains, and powders, with design criteria

© The Author(s) 2026
L. L. Kuan et al. (eds.), *Proceedings of the 2026 3rd International Symposium on Agricultural Engineering and Biology (ISAEB 2026)*, Advances in Biological Sciences Research 56,
https://doi.org/10.2991/978-94-6239-847-4_9

focused on discharge rate, blockage prevention, and mass-flow stability [3-7]. For living or fragile biological particles, however, the same flow improvement may be insufficient if it is accompanied by high wall impact or inter-particle compression. Recent applications of the discrete element method and multi-body dynamics to agricultural and aquaculture materials have demonstrated the value of simulation-based damage evaluation, but the coupling between hopper curvature and biological-particle damage remains insufficiently quantified[8-9].

To address this gap, this paper investigates the feeding hopper of an oyster seedling dispensing device through multi-sphere contact dynamics simulation. The study compares four typical hopper configurations, constructs a combined flow-and-damage evaluation framework, and further optimizes the central angle of the best-performing reverse-arc configuration. This work provides a theoretical basis and an engineering-feasible solution for low-damage grading and dividing equipment for oyster spat.

2 Materials and Methods

2.1 Hopper Geometry Configuration

Four hopper profiles were established for comparison: straight-wall, polyline, arc, and reverse-arc. The straight-wall hopper uses a linear contraction surface; the polyline hopper consists of two connected linear segments and therefore includes a geometric corner; the arc hopper has a convex curved contraction wall; and the reverse-arc hopper has a concave contraction wall. The inlet diameter, neck diameter, hopper body length, and neck tube length were kept constant at D = 150 mm, d = 60 mm, L1 = 80 mm, and L2 = 75 mm, respectively, so that the effect of wall configuration could be evaluated independently. The modeling results are shown in Fig. 1.

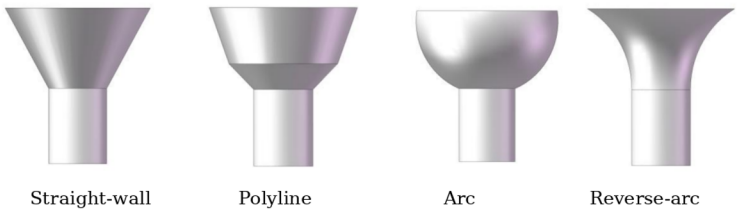


Fig. 1. Models of four hopper types.

2.2 Particle Equivalent Model and Initial Arrangement

Given that the actual oyster seed shells measure 15–25 mm in height and have irregular shapes, this study employs an equivalent smooth sphere with a diameter of dp = 20 mm for multi-body dynamics simulations to balance computational accuracy and efficiency. This simplification facilitates the investigation of how the macroscopic curvature of hopper walls influences collision-induced energy dissipation within the population—a

principle widely validated in bulk material mechanics simulations[10]. During the simulation, five spheres are released simultaneously above each hopper: one at the central axis (sphere ①), two near the left and right walls (spheres ② and ③), and two near the far left and right walls (spheres ④ and ⑤). All spheres are initially positioned 200 mm above the throat outlet with zero velocity, simulating free-fall entry of upstream material flow; their locations are shown in Fig. 2.

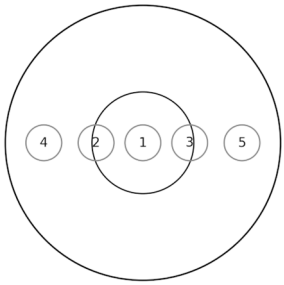


Fig. 2. Initial arrangement of the five equivalent spheres in the hopper inlet plane.

2.3 Contact Model and Simulation Parameters

The simulation employed the Hertz–Mindlin no-slip contact model to describe the normal and tangential contact forces for particle–particle and particle–wall interactions. A sphere was considered to have exited the hopper when its vertical coordinate decreased to zero. The initial velocity was set to 0 m/s, and the total simulation time was set to 0.3–0.4 s based on the actual falling process to ensure all particles passed completely through the throat region. The integration time step was set to 0.0005 s to capture the peak instantaneous collision force. Key contact parameters, based on Ref.[11]and practical conditions, are listed in Table 1.

Table 1. Simulation parameters.

Param	Stiffness	Power index	Damping	Depth	Density (kg/m^3)	Gravity (m/s^2)
Value	1000	2.2	0.1	0.1	1300	9.81

3 Results and Analysis

3.1 Effect of Different Configurations on Mass Flow Uniformity

To quantify the flow quality of the hopper configuration, this study introduces a temporal correction to Johanson's classical definition and improves the mass flow index (MFI) to simultaneously account for the temporal dispersion and velocity dispersion of particles reaching the outlet [12-13].

$$MFI = \frac{v_{min}}{v_{max}} \times \frac{t_{min}}{t_{max}} \quad (1)$$

where v_{min} and v_{max} are the instantaneous outlet velocities of the farthest wall particle and the central particle, respectively; t_{min} and t_{max} are the times at which the central particle and the farthest wall particle reach the outlet cross-section, respectively. An MFI closer to 1 indicates that the particle assembly approaches ideal "mass flow", with all particles descending synchronously and no dead zones or preferential flow channels.

The outlet times and outlet velocities of the central and near-wall particles were extracted from the simulations to quantify the flow uniformity of each hopper. Fig. 3 compares the characteristic values, and Table 2 lists the corresponding MFI values.

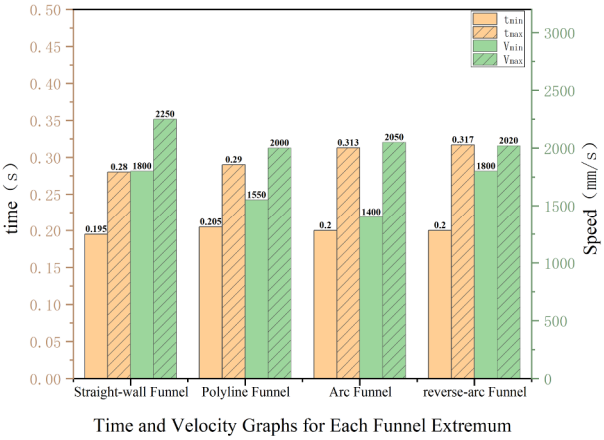


Fig. 3. Comparison of outlet-time and outlet-velocity extremes for the four hopper configurations.

Table 2. Overall flow indices and kinematic characteristic parameters corresponding to each hopper.

hopper Types	Tmin (s)	Tmax (s)	Vmin (mm/s)	Vmax (mm/s)	MFI
Straight-wall hopper	0.195	0.280	1800	2250	0.557
Polyline hopper	0.205	0.290	1550	2000	0.548
Arc hopper	0.200	0.313	1400	2050	0.437
Reverse-arc hopper	0.200	0.317	1800	2020	0.562

The reverse-arc hopper achieved the highest MFI, 0.562, indicating the best flow uniformity among the four designs. Its concave wall profile restrained excessive outward migration of near-wall particles and reduced the velocity difference between the central and boundary regions. The arc hopper produced the lowest MFI, 0.437, because the convex wall tended to drive particles toward the wall and enlarge the velocity gradient. The polyline hopper had an MFI close to that of the reverse-arc hopper, but its geometric corner introduced a local discontinuity that could increase collision risk. Therefore, flow uniformity alone is insufficient for selecting the optimal structure; collision-force indicators must also be considered.

3.2 Comprehensive Evaluation of Collision Damage Risk for Different Configurations

To comprehensively assess the suitability of the hopper structure for fragile biological particles, this study introduces a comprehensive damage index model D for multidimensional quantitative evaluation [8,14], defined as follows.

$$D = \sum_{i=1}^{n} \omega_i \cdot D_i^* \quad (2)$$

where D is the comprehensive evaluation index; ω_i is the weight coefficient of the i-th indicator; and D_i is the normalized indicator value.

Based on damage mechanics theory, the wall collision force F_W, the inter-particle collision force F_P, and the cumulative collision force on a single particle F_C are the three dominant factors causing shell damage, and their contributions are of the same order of magnitude [15]. A linearly weighted composite index with equal weights, expressed as.

$$D = 0.33 \times F_w^* + 0.33 \times F_P^* + 0.33 \times F_C^* \quad (3)$$

From the simulation results, the peak wall contact force, peak inter-particle contact force, and the maximum cumulative sum of collision forces exceeding 5 N sustained by any single sphere throughout the entire process were extracted for each hopper configuration. The corresponding D values were then calculated, and the results are presented in Table 3.

Table 3. Indicators of impact force and damage indices for each hopper.

Hopper type	F_W (N)	F_P (N)	F_C (N)	D
Straight-wall	29.281	18.437	46.1028	0.679
Polyline	33.834	15.521	59.4525	0.837
Arc	22.293	16.811	47.2129	0.398
Reverse-arc	22.375	7.223	35.0341	0.002

The reverse-arc hopper exhibited the lowest comprehensive damage index, D = 0.002. Its inter-particle collision force was 57.0% lower than that of the arc hopper, which shows that concave wall curvature can guide particles inward more smoothly and reduce throat-region compression. This result identifies the reverse-arc hopper as the best configuration in the first-stage comparison. However, its wall collision force at a 60° central angle was still 22.375 N, which may be risky for fragile spat after scale conversion. A further central-angle optimization was therefore necessary.

3.3 Optimization of the Reverse-Arc Hopper Central Angle and Mechanical Mechanism Analysis

The static compressive load associated with initial micro-cracking of 20 mm oyster spat is approximately 10-12 N, while complete crushing may occur at 13-28 N. Because brittle shells are more sensitive under impact loading, the effective impact-damage

force is lower than the static value. In this simulation, the equivalent sphere volume was approximately five times the volume of an actual spat; therefore, a simulated wall collision force above about 20 N was treated as an indicator of damage risk. The central angle θ of the reverse-arc hopper was varied from 45° to 75° in 5° increments while other dimensions were kept unchanged. The results are plotted in Fig. 4.

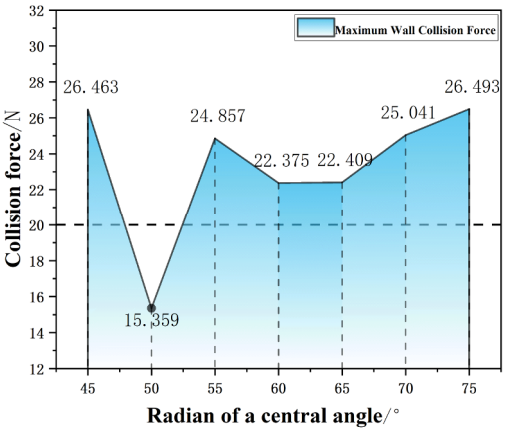


Fig. 4. Graphs showing the variation of maximum wall collision force for different central angles.

The evolution of the maximum collision force on the wall exhibits a typical "U-shaped" non-monotonic pattern: at θ = 45° it is 26.463 N; at θ = 50° it drops sharply to a global minimum of 15.359 N, a decrease of 42.0%; at θ = 55° it rebounds anomalously to 24.857 N; between θ = 60° and 65° it stabilizes at 22.3–22.4 N; and between θ = 70° and 75° it rises again to 25–26.5 N.

Mechanically, the descending segment from 45° to 50° can be explained by the longer sliding path and more gradual outlet tangent, which increase contact damping and reduce normal impact. When θ is increased beyond 50°, the curvature radius becomes too small, and the required centripetal acceleration rises. Particles are then more likely to detach from the wall and strike the throat section with a high normal velocity. The optimal angle must balance the benefit of a longer damping path against the risk of centrifugal detachment; the simulation results indicate that θ = 50° is the critical balance point.In accordance with the previously defined damage criterion, among the central angles ranging from 45° to 75°, only the 50° configuration, with a wall collision force of 15.359 N, falls significantly below the 20 N safety threshold. This corresponds to an actual impact force of approximately 3.1 N, which is well below the 4–5 N impact damage force for 20 mm oyster spat, providing a sufficient safety margin. At all other angles, the wall collision force exceeds 20 N, presenting a clear risk of collision-induced damage.

Consequently, the feeding hopper for the cage-dividing device is determined to be the reverse-arc hopper with a central angle of 50°.

4 Engineering Implications and Limitations

The combined MFI-D evaluation framework provides a practical way to screen hopper designs by considering both conveying smoothness and biological-particle protection. For the oyster seedling dispensing device studied here, the recommended design is a reverse-arc hopper with a 50° central angle. This configuration reduces simulated wall impact below the adopted risk criterion while maintaining relatively uniform outlet motion.

The study is nevertheless a simulation-based design assessment. The equivalent-sphere model simplifies real oyster-shell shape, surface roughness, moisture conditions, and shell-strength variability. Physical prototype tests should be conducted to validate the predicted damage reduction. In addition, future work should examine different oyster sizes, feed rates, material moisture levels, hopper-wall materials, and operating inclinations so that the robustness and practical applicability of the optimized design can be evaluated under realistic production conditions.

5 Conclusion

Focusing on the feeding hopper of an oyster spat grading device, this paper systematically investigates the influence of wall curvature direction on the flow uniformity and collision force field of particle assemblies using multi-sphere contact dynamics simulations, and optimizes the key geometric parameters of the preferred configuration.
The reverse-arc hopper gives the best performance (MFI = 0.562, D = 0.002), with inter-particle collision force 57 % lower than that of the arc type, due to the concave-wall centripetal effect that suppresses velocity gradients.

The optimal central angle is 50°, where the wall collision force reaches its minimum of 15.359 N; the U-shaped trend reflects the trade-off between damping dissipation and centrifugal detachment.

The combined MFI-D method balances flow uniformity and damage reduction, and the optimised parameters offer a practical reference for low-damage design of aquaculture seed conveyors.

Acknowledgments

This work was supported by the Shandong Provincial Rural Revitalization Science and Technology Innovation Boosting Action Plan Project (Grant No. 2025TZXD033).

Disclosure of Interests

The authors have no competing interests to declare that are relevant to the content of this article.

References

1. M. M. Helm, N. Bourne, and A. Lovatelli: Hatchery Culture of Bivalves: A Practical Manual. FAO Fisheries Technical Paper No. 471, Food and Agriculture Organization of the United Nations, Rome (2004).
2. Scherer, A. E., Smee, D. L.: Eastern oysters Crassostrea virginica produce plastic morphological defenses in response to crab predators despite resource limitation. The Biological Bulletin 233(2), 144-150 (2017).
3. Miyauchi Y, Yoshida M, Shirakawa Y. Discrete element method analysis of the relationship between flow pattern and particle discharge rate in a micro hopper[J].Advanced Powder Technology,2024,35(6)104465-.DOI:10.1016/J.APT.2024.104465.
4. Huang T, Wu B, Xie F, et al. Characterisation of discharge and flow rate predictions for asymmetric wedge-shaped hoppers[J].Biosystems Engineering,2024,24596-105. DOI:10.1016/J.BIOSYSTEMSENG.2024.07.007.
5. Hadi A, Shi H, Pang Y, et al.Identification of dominant DEM parameters for multi-component segregation during heap formation, hopper discharge and chute flow[J].Powder Technology,2024,444119985-119985.DOI:10.1016/J.POWTEC.2024.119985.
6. Changhao G, Kaiqiang Y, Youlin X, et al.Discharge characteristics of conical and hyperbolic hoppers based on discharge time distribution[J].Powder Technology,2023,426 DOI:10.1016/J.POWTEC.2023.118665.
7. Feiyang C, Yidong X, Jordan K, et al. Hopper discharge flow dynamics of milled pine and prediction of process upsets using the discrete element method[J].Powder Technology,2023,415 DOI:10.1016/J.POWTEC.2022.118165.
8. Opara, L. U., Pathare, P. B.: Bruise damage measurement and analysis of fresh horticultural produce--a review. Postharvest Biology and Technology 91, 9-24 (2014). https://doi.org/10.1016/j.postharvbio.2013.12.009
9. Shan Jianjun, Guan Chongwu, Song Hongqiao, et al. Evaluation of Damage Caused by Fish Pump Based on Principal Component Analysis[J].Chinese Agricultural Science Bulletin,2021,37(29)140-145
10. Ketterhagen R W, Curtis S J, Wassgren R C, et al.Predicting the flow mode from hoppers using the discrete element method[J].PowderTechnology,2009,195(1):1-10. DOI:10.1016/j.powtec.2009.05.002.
11. Yuan, L., Lu, J., Miao, C., et al.: Dynamic properties of oyster shells based on a fractional-order model. Explosion and Shock Waves 43(1), 3-17 (2023). https://doi.org/10.11883/bzycj-2022-0318
12. Siqiang W, Zhijun W, Shunying J .Investigation of the flow characteristics of spherical harmonic particles using the level set method[J].Powder Technology,2023,413 DOI: 10.1016/J.POWTEC.2022.118069.
13. Wu H, Wang Y, Liu S, et al.Macro and microscopic analysis of granular flow in curved hoppers[J].Powder Technology,2024,443119855-.DOI:10.1016/J.POWTEC.2024.119855.
14. Xingjian H, Qijun Z, Dedao L, et al.A design method of hopper shape optimization with improved mass flow pattern and reduced particle segregation[J].Chemical Engineering Science,2022,253 DOI:10.1016/J.CES.2022.117579.
15. Liu, W., Xu, J., Liu, X.: Numerical study on collision characteristics for non-spherical particles in venturi powder ejector. Vacuum 131, 285-292 (2016). https://doi.org/10.1016/j.vacuum.2016.07.006

Open Access This chapter is licensed under the terms of the Creative Commons Attribution-NonCommercial 4.0 International License (http://creativecommons.org/licenses/by-nc/4.0/), which permits any noncommercial use, sharing, adaptation, distribution and reproduction in any medium or format, as long as you give appropriate credit to the original author(s) and the source, provide a link to the Creative Commons license and indicate if changes were made.

The images or other third party material in this chapter are included in the chapter's Creative Commons license, unless indicated otherwise in a credit line to the material. If material is not included in the chapter's Creative Commons license and your intended use is not permitted by statutory regulation or exceeds the permitted use, you will need to obtain permission directly from the copyright holder.

